ACKNOWLEDGMENTS

The authors would like to thank Roy Bailey and Bob Jachens of the USGS for many fruitful discussions and Carle Otte and Dick Dondanville of Unocal Geothermal for making the Unocal gravity data

REFERENCES

Abers, G., 1985. The subsurface structure of Long Valley caldera, Mono County, California. J. Geophys. Res., v. 90, p. 3527–3638.

Bailey, R.A., Dalrymple, G.B., and Lanphere, M.A., 1976. Volcanism, structure, and geochronology of Long Valley caldera, Mono County, California. J. Geophys. Res.. v. 81, p. 725–744.

Bailey. R.A., and Koeppen, R.P., 1977. Preliminary Geologic map of Long Valley caldera. U.S. Geol. Survey Open-File Map 77–468.

Bailey. R.A., 1987. Relationship between basement geology, faults and volcanic vents, Long Valley caldera, eastern California. *In* N.E. Goldstein (ed.). Proceedings, Symposium on the Long Valley Caldera: A Pre-Drilling Data Review. Lawrence Berkeley Laboratory Report LBL-23940. p. 1–7.

Carle. S.F.. 1987. Three-dimensional gravity modeling of the geologic structure of Long Valley caldera (MS. thesis). University of California, Berkeley. Lawrence Berkeley Laboratory Report LBL-23538.

Cordell, L., and Henderson, R.G., 1968. Iterative three-dimensional solution of gravity anomaly **data** using a digital computer. Geophysics, v. 33. p. 596–601.

Dawson, P.B., Iyer, H.M., and Evans, J.R., 1987. Structure of crust and upper mantle in the Long Valley, California region as determined from teleseismic travel-time residuals. *In* N.E. Goldstein (ed.), Proceedings, Symposium on the Long Valley Caldera: A Pre-Drilling Data Review. Lawrence Berkeley Laboratory Report LBL-23940, p. 54–62.

Eichelberger, J.C., Younker, L.W., Vogel, T.A., and Miller, C.D., 1988. Structure and stratigraphy beneath a young phreatic vent; South Inyo Crater, Long Valley caldera, California. J. Geophys. Res. (in press).

Hill, D.P., Kissling, E., Luetgert, J.H., and Kradolfer, N., 1985. Constraints on the upper crustal structure of the Long Valley–Mono Craters volcanic complex, eastern California from seismic refraction measurements. J. Geophys. Res., v. 90, p. 11135–11150.

Johnson, R.W., 1969. Volcanic geology of Mount Suswa, Kenya. Philos. Trans. R. Soc. London, v. 265, p. 383–412.

Kane, M.F., 1962. A comprehensive system of terrain corrections using a digital computer. Geophysics, v. 27, no. 4, p. 455–462.

Kane, M.F., Mabrey, D.R., and Brace, R., 1976. A gravity and magnetic investigation of the Long Valley caldera, Mono County, California. J. Geophys. Res., v. 81, p. 754–762.

Lachenbruch, A.H., Sass, J.H., Munroe, R.J., and Moses, Jr., T.H., 1976. Geothermal setting and simple heat conduction models for the Long Valley caldera. J. Geophys. Res., v. 81, p. 769–784.

Suemnicht, G.A., and Varga, R.J., 1987. Constraints on models of structures and hydrothermal circulation in Long Valley, California. *In* N.E. Goldstein (ed.), Proceedings, Symposium on the Long Valley Caldera: A Pre-Drilling Data Review. Lawrence Berkeley Laboratory Report LBL-23940, p. 32–38.

Multicomponent VSPs at Cajon Pass and the Salton Sea

*T.M. **Daley,** T.V. McEvilly, and E.L. Majer*

The Vertical Seismic Profile (VSP) is a proven tool for studying the seismic-wave properties near a well and detailing subsurface structure (Hardage, 1985; Oristaglio, 1985). The usefulness of the VSP method has been increased by the acquisition of multicomponent data using a three-component borehole geophone in conjunction with both P-wave and *S*-wave seismic sources. The three-component geophone allows recording of the entire wavefield, and the *S*-wave source (usually a seismic vibrator truck) allows control of the shear-wave polarization. Among the possible **uses** of these data are fracture

detection and characterization via seismic anisotropy measurements (Crampin, 1985; Majer et al., 1988). The application of multicomponent VSP data is seen in two surveys conducted by Lawrence Berkeley Laboratory (LBL) and analyzed at LBL's Center for Computational Seismology (CCS). First was the Salton Sea VSP (SSVSP), acquired at the Salton Sea scientific well in southern California's Imperial Valley; the other was the Cajon Pass VSP (CJVSP) at the Cajon Pass scientific well near the San Andreas fault in southern California. Both surveys made use of LBL's seismic shear-wave vibrators to obtain shear-wave surveys along with the more standard *P*-wave surveys. Use of a three-component geophone, along with careful rotation of the recorded data traces into a,,wavefront-based coordinate system, allowed analysis of many aspects of the seismic-wave propagation properties around the wells.

At the Salton Sea well, located near the Salton Sea geothermal field, standard VSP analysis techniques were used to identify reflecting horizons both within the survey interval (from 457 to 1737 m) and deeper in the well (Fig. 1). The reflection at 2100 m in Fig. 1 is associated with a fractured reservoir, and event C is interpreted as a scattered wave from a fracture zone near the well at a depth of 900 m. One goal of the SSVSP was location of fracture zones that are associated with the geothermal process. Seismic-velocity anisotropy and the associated shear-wave splitting are indicators of fracturing utilized in the SSVSP analysis. Travel-time differences observed between orthogonal polarizations of the shear-wave source, labeled *SV* and *SH*, show a variation in anisotropy with depth. The *SV* source motion is polarized in the radial direction toward the well, and the *SH* source motion is polarized transverse to the radial. In an isotropic material, these polarizations will generate the standard *SV*- and *SH*-type shear waves. Since the travel time is measured on a component with the same polarization as the source, travel-time difference is a measurement of shear-wave velocity anisotropy,

Three-component particle-motion analysis of shear-wave arrivals was found to be an effective method for characterizing the subtleties in the *S*-wave splitting throughout the various zones in the well. Although the travel-time measurements show anisotropy of only around 1%, the particle-motion analysis showed clear definition of changes in the *S*-wave propagation characteristics. Figure 2 shows the particle motion at 580 m, where the data are in the rotated, wavefront-based coordinate system of radial, *SH*, and *SV* components and plotted as three 2-dimensional cross sections on the faces of a cube

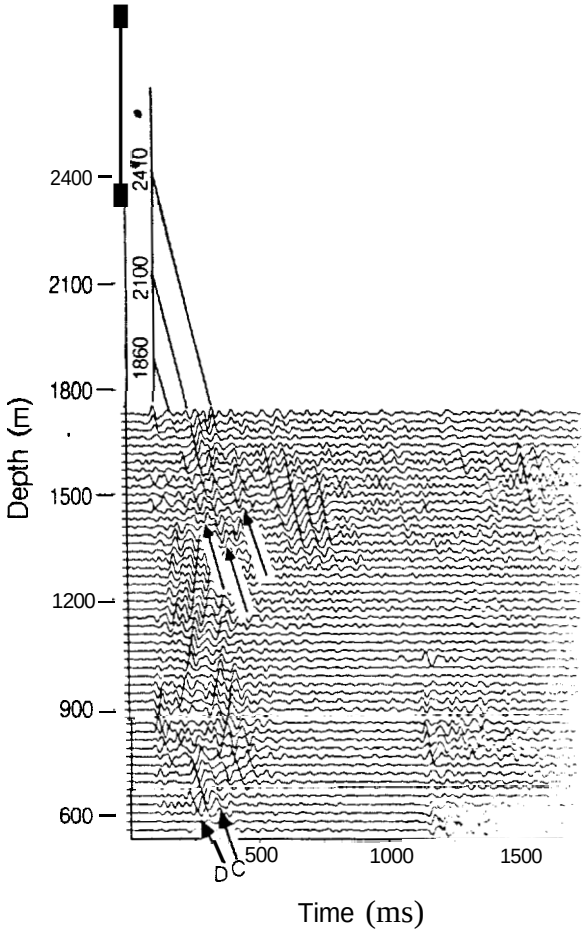

Figure 1. Reflector depth estimation for far-offset *P*-source, vertical component. Section is time-shifted to align first arrivals and dip-filtered to attenuate downgoing energy. Three deep events are identified with generation depths estimated at 1860, 2100, and 2410 m. Event D is a *P*-wave reflection from 850 m. Event C is a vertically scattered *P*-wave event. The different moveout of events D and C indicate different modes of generation. [XBL 884-10168]

(Daley, 1987; Majer et al., 1988). This linear motion is typical of that expected for isotropic propagation. Changes in particle motion associated with propagation in anisotropic material are easily seen on this type of three-component hodograph.

In the CJVSP survey, the shear-wave vibrator occupied one offset position for three runs of the borehole geophone, allowing three different *S*-wave polarizations to be obtained. These polarizations were radial and transverse to a line from the well, and the intermediate orientation, and were called *SV*, *SH*, and *S*45, respectively. Complete data sets were obtained for the SV and *SH* polarizations (from surface to 1800 m, with 10-m spacing), but the third run was not finished, giving coverage with the *S*45

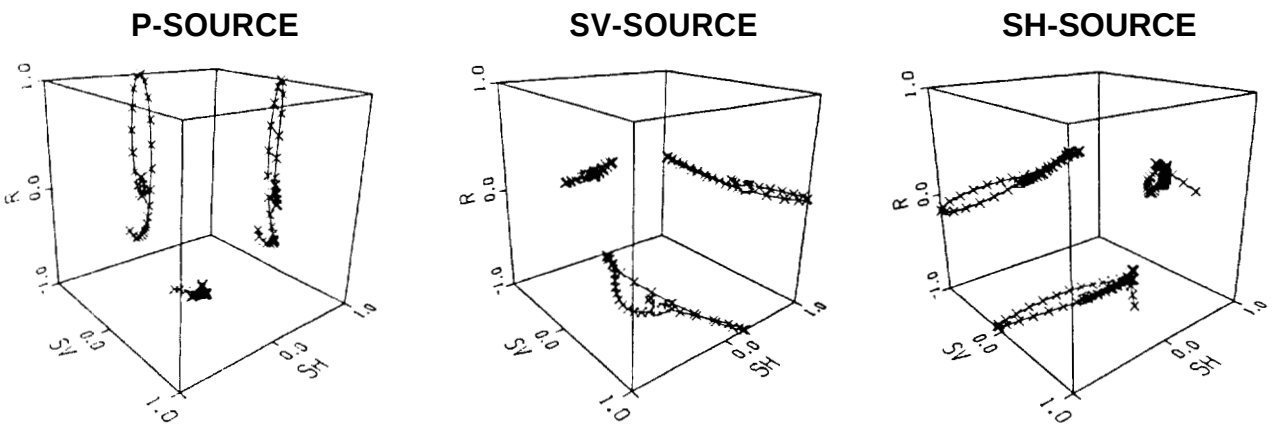

Figure 2. Three-component particle-motion hodographs for all three far-offset sources at 580 m recording depth. Plotted points are 2 ms apart. Each axis of the cube displays one component of motion, giving three 2-D projections. Purely isotropic S-wave propagation would produce linear trajectories in the *SV-SH* plane shown on the cube's bottom. [XBL 877-3164A]

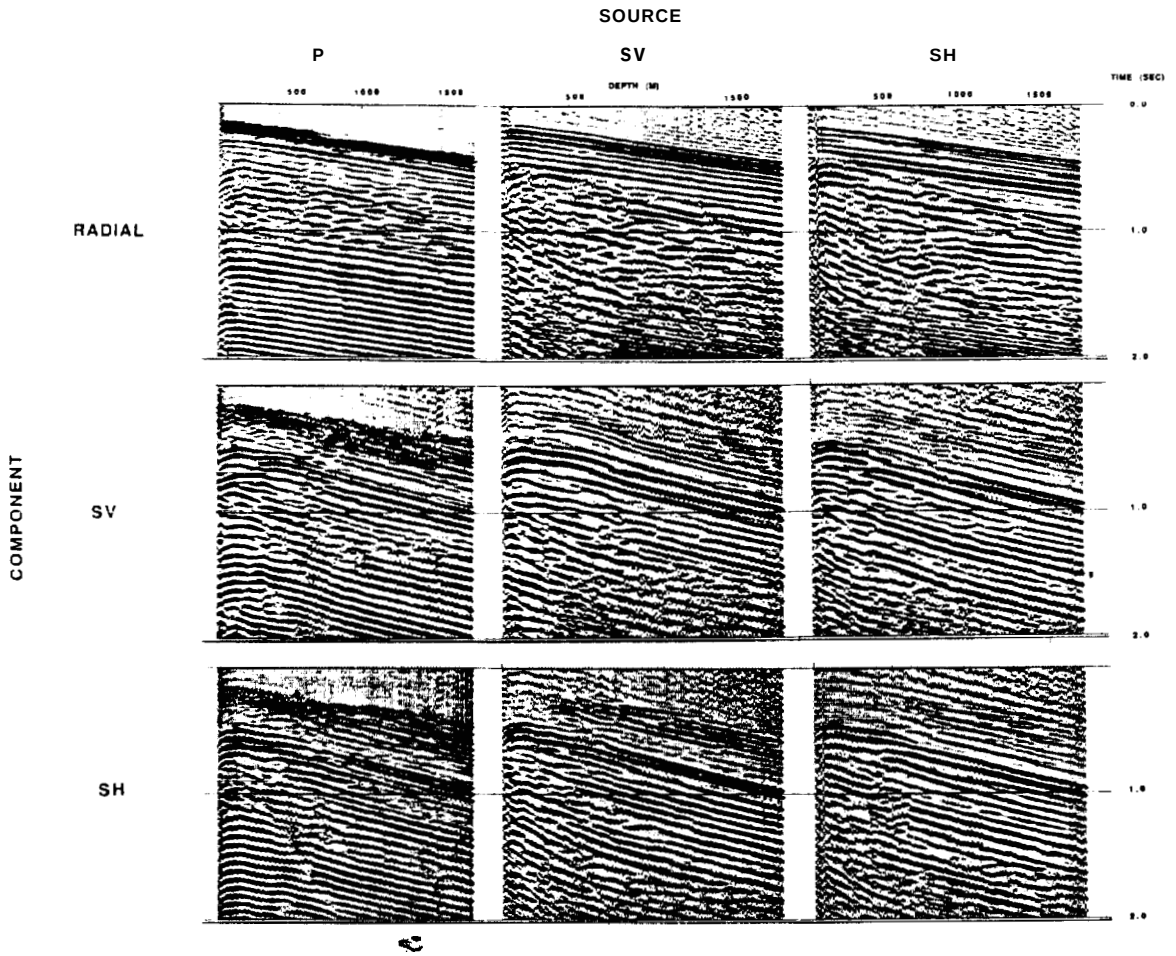

Figure 3. Nine-component display of Cajon Pass **VSP** data. Each section **is** a depth versus time display of the data from one source type (*P*, *SH*, or *SV*) recorded on one geophone component (radial, *SH*, or *SV*). The data have been rotated into radial, ***SH***, and *SV* components from the original, randomly rotated geophone recordings using the first *P*-wave arrival. [XBL 8710-4019]

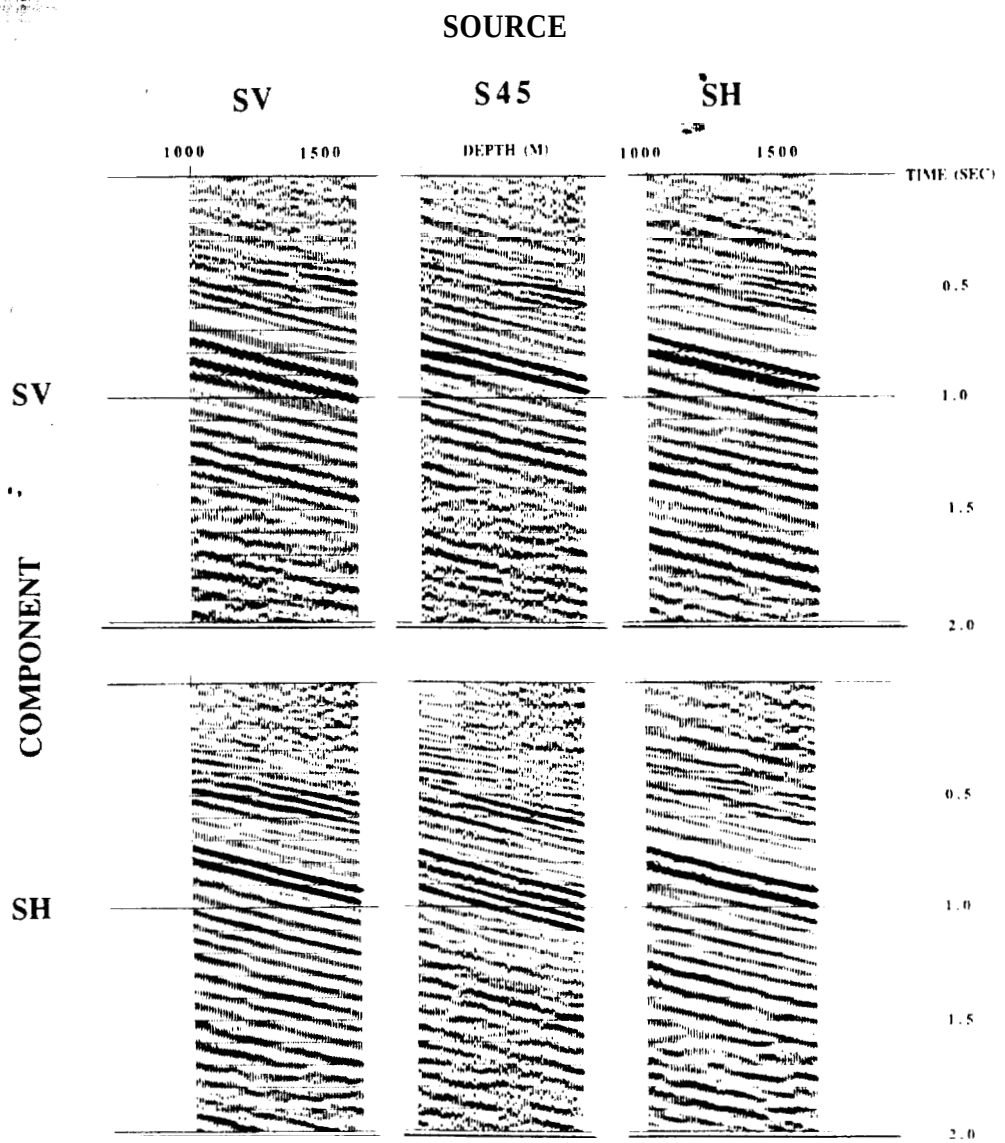

Figure 4. Shear-wave data from Cajon Pass VSP. The *SV*, *SH*, and *S*45 sources are three polarizations of a shear-wave vibrator. The borehole geophone data have been rotated into *SH* and *SV* components. The variation in observed arrivals between sources can be used to study seismic anisotropy. [XBL 8712-5118]

source from 1040 to 1630 m. By rotating the data from the *P*, *SV*, and *SH* sources into the radial, *SH*, and *SV* components, a nine-component display could be produced for the CJVSP (Fig. **3).** The variation of events seen on each of these nine components shows the details that multicomponent VSPs produce compared to standard VSPs, which have one source and one receiver component (such as the P-source, radial-component data shown in Fig. **3).** In the CJVSP there is a significant interface near 500 m between the Punchbowl sedimentary formation and the granitic basement rock. The effect of this contact is seen in the breakup of the first shear-wave arrival near 0.5 s on the *SV* and *SH* components of the *SV* and *SH* sources. The contact is also delineated by the mode-convened shear waves seen on the *SV* and *SH* components of the *P* and *SV* sources at 0.25 s.

The three shear-wave data sets are shown in Fig. **4** for the *SH* and *SV* component data. Anisotropic effects are clearly seen on the *SH* components, where the *S*45-generated amval between 0.7 and 1.1 s has a split waveform and a less coherent arrival The affect of this anisotropy is seen on two-component panicle-motion plots in Fig. 5. The nearby San Andreas fault is expected to caus

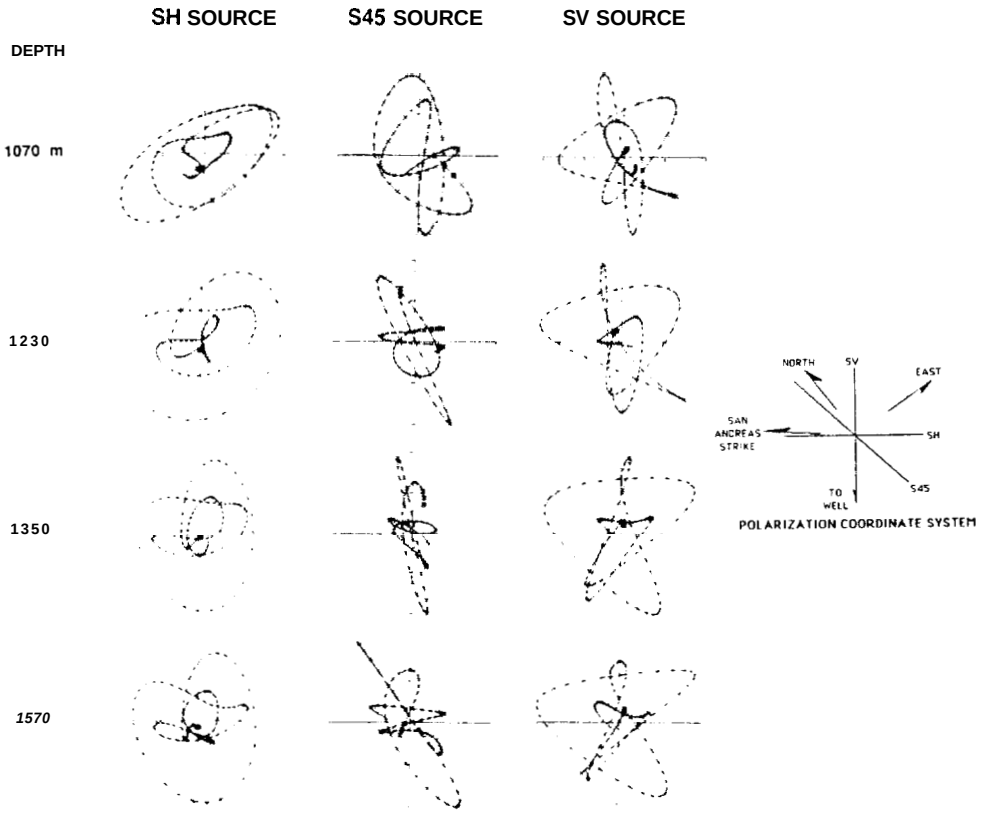

Figure 5. Two-component panicle motion of shear-wave arrivals at depths from 1070 to 570 m for three polarizations of the shear source. The vertical axis of each plot **is** motion on the *SV* component, and the horizontal axis is motion on the *SH* component. Each data point is 2 ms apart in time, and the first three points are circled to identify first motion. The side plot shows the orientation of each source and axis with respect to north. and with respect to the strike direction of the San Andreas fault. [XBL 8712-5272]

microfracturing, which will affect the orientation of the shear-wave particle motion. In Fig. **5**, the *S*45- and SV-generated arrivals have a component of motion in the fault direction, but the *SH*-generated amval, which is aligned with the fault, does not stay linear as we would expect. This type of particle-motion analysis of the CJVSP data shows that factors other than the San Andreas fault are affecting the seismic anisotropy.

REFERENCES

Crampin, *S.*, 1985. Evaluation of aniotropy by shear-wave splitting. Geophysics, v. *50*, no. 1, p. **142–**152.

Daley, T.M., 1987. Analysis of ***P-*** and *S*-wave **VSP** data from the Salton Sea geothermal field (M.S. thesis). University of California, Berkeley. Lawrence Berkeley Laboratory Report LBL-24661.

Hardage, B.A., 1985. Vertical Seismic Profiling—Part A: Principles. Geophysical Press Limited, London, p. 337–340.

Majer, E.L., McEvilly, T.V., Eastwood, F., and Myer, L., 1988. Fracture detection using ***P-*** and S-wave VSPs at the geysers geothermal field. Geophysics, v. **53,** no. 1, p. 76–84.

Oristaglio, M.L., 1985. **A** Guide to the current uses of vertical seismic profiles. Geophysics, v. 50, **no. 12, p.** 2473.